AIAA JOURNAL
Vol. 36, No. 5, May 1998

Mesh Refinement and Modeling Errors in Flow Simulation

Antony Jameson* and Luigi Martinelli†
Princeton University, Princeton, New Jersey 08544

This paper presents a perspective on verification and validation of computational fluid dynamics tools for analysis and design. It identifies principal sources of error due to approximations in the physical model, numerical discretization, and implementation. Issues in algorithm design and tradeoffs between modeling accuracy and computational costs are discussed. Computational examples are drawn from the authors' work.

I. Introduction

THE simulation of fluid flow involves two essential steps: 1) the definition of a suitable mathematical model that describes the physical system of interest, and 2) the development and implementation of numerical techniques to compute a solution of the mathematical model using digital computers. Both steps generally introduce approximation in the simulation, and the resulting errors should be independently understood and possibly quantified. Thus, the validation of computational methods is not simply a matter of comparing numerical results with experimental data. One must begin by establishing that the mathematical model is logically consistent and that it is approximated by a correct numerical method, which is in turn implemented in a correct computer program. Only then can a comparison with experimental data be used to determine whether the mathematical model incorporates enough of the true physics to make useful predictions for the purpose in hand.

If it is first established, for example, that a numerical method accurately solves the incompressible potential flow equations, then comparisons with experimental data can be used to determine whether this model adequately represents any real flows. Separated viscous flows clearly do not satisfy the assumptions used in the derivation of the potential flow equation. Thus, the failure of the method to predict these flows would be perfectly consistent with the assumptions embedded in the method and would not necessarily invalidate the use of the method to predict flows for which the assumptions are reasonably close to being satisfied. In fact, potential flow models have been successfully used to predict a wide variety of attached flows at low Mach numbers.

With this understanding, it is apparent that each step in the process of developing the final complete software needs to be independently verified in every feasible way. First the assumptions of the formulation of the mathematical model need to be clearly defined and understood, and the logical consistency of the model needs to be verified. This includes the formulation of proper boundary conditions and ideally proof that a solution exists and is both unique and well posed, depending continuously on the data. Next, it is necessary to derive a correct numerical approximation and to verify both its consistency with the mathematical model and its accuracy. Finally, one must try to establish that the implementation of the method in a computer program is correct.

The choice of an appropriate mathematical model represents a tradeoff between the accuracy required in the simulation and the computational complexity and cost. Nonlinearities and a disparity of length and time scales control many critical phenomena of fluid flow. For example, whereas the actual thickness of a shock wave is on the order of a mean free path of the gas particles, on a macroscopic scale its thickness is essentially zero. In turbulent flow, energy is transferred from large-scale motions to progressively smaller eddies until the scale becomes so small that the motion is dissipated by viscosity. The ratio of the length scale of the global flow to that of the smallest persisting eddies is of the order $Re^{3/4}$, where Re is the Reynolds number, typically in the range of 30×10^6 for an aircraft and even larger for naval applications. To resolve such scales in all three space directions, a computational grid with the order of $Re^{9/4}$ cells would be required. This is beyond the range of any current or foreseeable computer. Consequently mathematical models with varying degrees of simplification have to be introduced to make computational simulation of flow feasible and to produce viable and cost-effective methods, and it is necessary to understand and to quantify the errors that originate from these simplifications.

Efficient flight is generally achieved by the use of smooth and streamlined shapes that avoid flow separation and minimize viscous effects, with the consequence that useful predictions can be made using inviscid models. The elimination of viscous effects allows the assumption of irrotational flow, which leads to Laplace's equation for incompressible flow, and the linearized supersonic flow equation for high-speed flow past slender bodies. Although simplified models of this type can be very useful in applications that are close to satisfying the underlying assumptions, they are completely invalid for complex viscous flows. At an intermediate level of complexity are the nonlinear inviscid models, including the transonic potential flow equation and the Euler equations. The logical verification of these simplified models belongs to the field of classical fluid dynamics. They have been extensively used in aircraft design and thus validated by several independent studies. However, the full viscous equations are likely to be needed for the simulation of arbitrary complex separated flows, which occur in several practical devices: high-angle-of-attack aircraft, high lifting devices, multistage compressors and turbines, and maneuvering submarines and ships. To treat these kinds of flow at high Reynolds numbers, one is generally forced to estimate turbulent effects by Reynolds averaging of the fluctuating components. This requires the introduction of a turbulence model.

Computational fluid dynamics (CFD) methods for high-Reynolds-number viscous flow are still not validated as one would like before their use in the design process. The fidelity of modeling of high-Reynolds-number viscous flows continues to be limited by computational costs and, for separated flows, by inadequate turbulence modeling. In this case it becomes difficult to distinguish between the errors due to the mathematical model and those caused by the discretization, and care must be taken to isolate the cause of discrepancy either in the mathematical model or in the numerical scheme. Grid refinement studies are instrumental for eliminating uncertainties and errors attributable to the numerical scheme.

The selection of sufficiently accurate mathematical models and a judgment of their cost effectiveness ultimately rests with industry. Aircraft and spacecraft designs normally pass through the three phases of conceptual design, preliminary design, and detailed design. Correspondingly, the appropriate CFD models will vary in complexity. In the conceptual and preliminary design phases, the emphasis will be on relatively simple models that can give results with very rapid turnaround and low computer costs to evaluate

Presented as Paper 96-2050 at the AIAA 27th Fluid Dynamics Conference, New Orleans, LA, June 17–20, 1996; received Oct. 22, 1996; revision received Feb. 10, 1998; accepted for publication Feb. 11, 1998.

*James S. McDonnell Distinguished University Professor of Aerospace Engineering, Department of Mechanical and Aerospace Engineering. Fellow AIAA.

†Assistant Professor, Department of Mechanical and Aerospace Engineering. Member AIAA.

alternative configurations and to perform quick parametric studies. The detailed design stage requires the most complete simulation that can be achieved with acceptable cost. Once the selection of a mathematical model has been made, one is faced with the task of devising appropriate numerical methods that solve a discrete representation of the analytical model.

For a numerical method, internal and logical verification require proof that discretization and round-off errors can be bounded and that, in principle, the numerical method will compute an accurate solution of the mathematical model with small enough mesh width and sufficient precision. For example, we may prove that the error approaches zero as some power of the mesh width assuming exact arithmetic, and we may also verify this by numerical experiments. For a properly posed initial value problem, classical numerical analysis techniques can be used for verification (including both consistency and proof of convergence) of a numerical method. In practice, however, the nonlinearity of the conservation laws and the geometric complexity of the flow domain of interest in most applications make it difficult to devise elegant analytical tools for studying the properties of a numerical scheme. Thus, although the principles underlying the design and implementation of robust schemes that can accurately resolve the inviscid conservation laws for compressible flows are now quite well established, mesh refinement remains the most obvious and successful technique available for verifying the level of accuracy of the scheme. For time-resolved calculations, a similar grid-refinement study must be performed by computing with a sequence of time steps to infer the level of time accuracy of the calculations.

Furthermore, it is necessary to seek a confirmation that the actual implementation in software converges to a correct answer when the mesh width and the time step are sufficiently small. A correct answer may be supplied as independent solutions of the model, either analytical (for special cases) or by independently developed numerical methods. Verification and validation of the implementation of the method in a computer program are difficult tasks, especially in the case of complex software. It may be very hard to detect an error, for example by a factor of 2, in some parameter that only has a small influence on the results. In the authors' experience it pays to divide the complete program into relatively small submodules. Then one or more alternate implementations of the submodels should be independently coded, and it should be verified that each alternate implementation can be substituted in the complete software while producing the same final results within roundoff errors. Finally, the confidence level in the correctness of computer programs can be increased by comparisons with other computer programs that are intended to represent the same model, provided that the results agree.

Once the mathematical model, the numerical discretization, and its implementation have been independently verified, the final validation of the simulation process can be carried out by comparing the results predicted by the simulation with independent empirical data.

This paper describes the verification and validation process of numerical algorithms for flow simulations by discussing two examples drawn from the authors' work.

II. Verification and Validation of CFD Algorithms

This section presents two examples of verification and validation of computational methods drawn from some recent work by the authors. We first discuss the progression of steps taken for validating the H-CUSP (H-convective upwind and split pressure) scheme for both inviscid and viscous steady compressible flow. Then, we present some of the essential elements of a verification and validation study of an efficient multigrid dual time-stepping method for computing time-resolved incompressible flow.

Validation of a CFD Algorithm for the Transonic Regime

A theory describing the discrete shock structure of a variety of schemes that introduce upwind biasing by matrix diffusion has been developed by Jameson.[1,2] These include the E-characteristic scheme, which is equivalent to Roe's flux difference splitting,[3] the H-characteristic scheme, which exactly preserves constant total enthalpy in steady flow, and the E and H-CUSP schemes. In particular, the H-CUSP scheme appears to offer favorable tradeoffs for the simulation of complex compressible flows. The following sections describe a hierarchy of steps that have been used by the authors to validate the H-CUSP scheme, from the verification of the discrete shock structure predicted by theory to the validation of the method for three-dimensional turbulent flows.

Table 1 Shock wave at Mach 20: H-CUSP scheme

I	ρ	u	p	M	s
12	1.0000	23.6643	1.0000	20.0000	0.0000
13	1.0000	23.6643	1.0000	20.0000	0.0000
14	1.0000	23.6643	1.0000	20.0000	0.0000
15	1.0000	23.6643	1.0000	20.0000	0.0000
16	1.0000	23.6643	1.0000	20.0000	0.0000
17	1.0000	23.6643	1.0000	20.0000	0.0000
18	1.0000	23.6643	1.0000	20.0000	0.0000
19	1.0000	23.6643	1.0000	20.0000	0.0000
20	1.0000	23.6643	1.0000	20.0000	0.0000
21	1.0000	23.6643	1.0000	20.0000	0.0000
22	4.1924	7.3248	307.4467	0.7229	40.3353
23	5.9259	3.9935	466.4889	0.3804	37.6355
24	5.9259	3.9935	466.4889	0.3804	37.6355
25	5.9259	3.9935	466.4889	0.3804	37.6355
26	5.9259	3.9935	466.4889	0.3804	37.6355
27	5.9259	3.9935	466.4889	0.3804	37.6355
28	5.9259	3.9935	466.4889	0.3804	37.6355
29	5.9259	3.9935	466.4889	0.3804	37.6355
30	5.9259	3.9935	466.4889	0.3804	37.6355
31	5.9259	3.9935	466.4889	0.3804	37.6355
32	5.9259	3.9935	466.4889	0.3804	37.6355

One-Dimensional Shock

To verify the discrete structure of stationary shocks predicted by the theory, calculations were performed for a one-dimensional problem with initial data containing left and right states compatible with the Rankine–Hugoniot conditions. An intermediate state consisting of the arithmetic average of the left and right states was introduced at a single cell in the center of the domain. With this intermediate state the system is not in equilibrium, and the time-dependent equations were solved to find an equilibrium solution with a stationary shock wave separating the left and right states. Table 1 shows the results for a shock wave at Mach 20 for the H-CUSP scheme. The SLIP (symmetric limited positive) construction was used with a soft limiter. The table shows the values of ρ, u, p, M, and the entropy $S = \log(p/\rho\gamma) - \log(p_L/\rho_L^\gamma)$. The scheme displays a perfect one-point shock structure. The entropy is zero to four decimal places upstream of the shock, and is constant to four decimal places downstream of the shock. There is a slight excursion of the entropy at the interior point in the results for the H-characteristic and H-CUSP schemes. Table 1 also verifies that the SLIP construction produces solutions that are entirely devoid of oscillations both upstream and downstream of the shock wave and that it does not spread out the shock structure at all.

Airfoil Calculations

The results of transonic flow calculations using the H-CUSP scheme are illustrated in Figs. 1 and 2. The final stagnation enthalpy is exactly constant, in accordance with the theory. The H-CUSP scheme was simplified by replacing the Roe averages by arithmetic averages.

Calculations are presented for two well-known airfoils, the RAE 2822 and the NACA 0012. The equations were discretized on meshes with O-topology extending out to a radius of about 100 chords.

In each case the calculations were performed on a sequence of successively finer meshes from 40×8 to 320×64 cells, while the multigrid cycles on each of these meshes descended to a coarsest mesh of 10×2 cells. Figures 1 and 2 show the final results for each scheme on 320×64 meshes for the RAE 2822 airfoil at Mach 0.75 and 3-deg angle of attack and for the NACA 0012 airfoil at Mach 0.8 and 1.25-deg angle of attack and also at Mach 0.85 and 1-deg angle of attack. For the three cases the pressure distribution is displayed after a sufficient number of cycles for its convergence. The extended

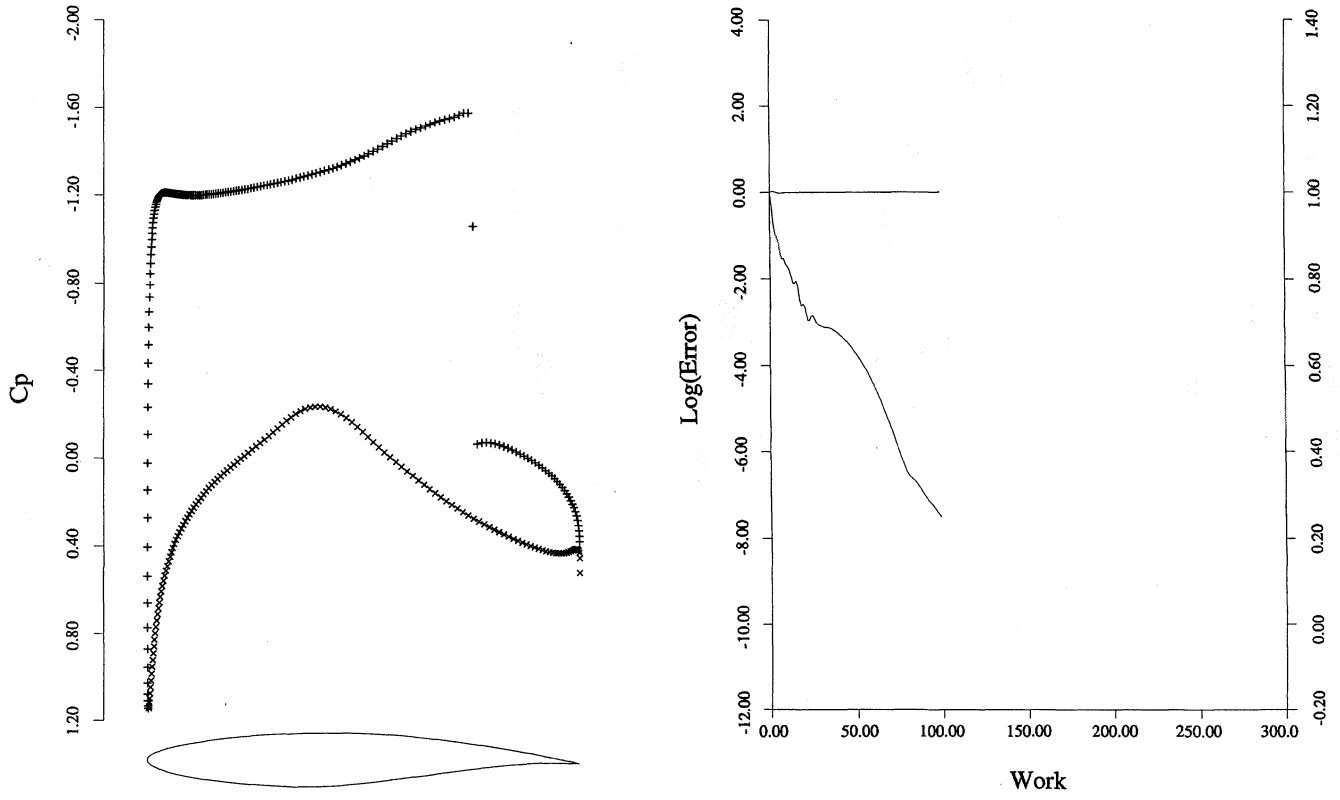

a) C_p after 25 cycles: C_l = 1.1312 and C_d = 0.0469

b) Convergence

Fig. 1 RAE 2822 airfoil at Mach 0.750 and α = 3.0 deg: H-CUSP scheme.

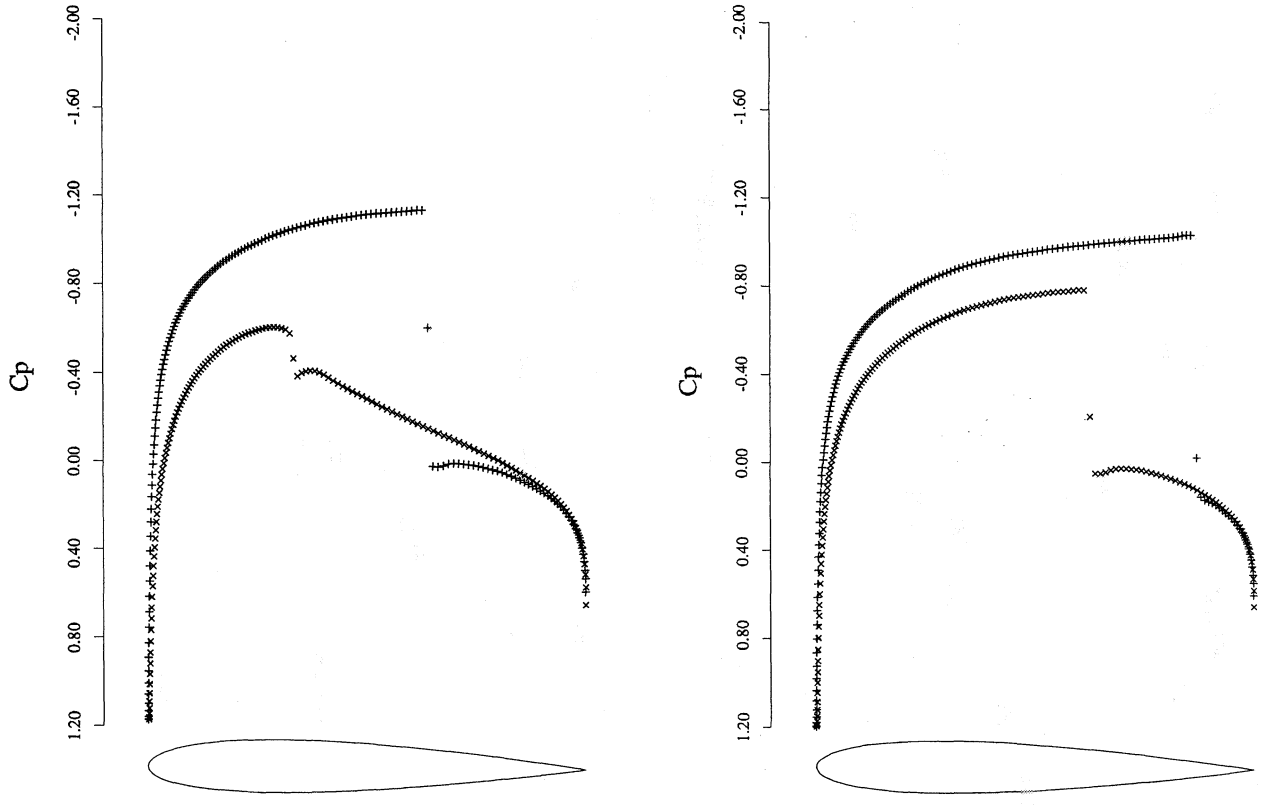

a) C_p after 35 cycles: Mach 0.8, α = 1.25 deg, C_l = 0.3654, and C_d = 0.0232

b) C_p after 35 cycles: Mach 0.85, α = 1 deg, C_l = 0.3861, and C_d = 0.0582

Fig. 2 NACA 0012 airfoil: H-CUSP scheme.

Table 2 Drag coefficient on a sequence of meshes: H-CUSP scheme

Mesh	RAE 2822 Mach 0.50, $\alpha = 3$ deg	NACA 0012 Mach 0.50, $\alpha = 3$ deg	Korn airfoil Mach 0.75, $\alpha = 0$ deg
40×8	0.0062	0.0047	0.0098
80×16	0.0013	0.0008	0.0017
160×32	0.0000	0.0000	0.0000

convergence history presented for the RAE 2822 calculation provides a verification that the solution process will reach a true steady state, with residual errors that can be reduced to machine zero within roundoff error, if it is continued for a sufficient number of cycles. In the pressure distributions the pressure coefficient $C_p = (p - p_\infty)/(\frac{1}{2}\rho_\infty q_\infty^2)$ is plotted with the negative (suction) pressures upward, so that the upper curve represents the flow over the upper side of a lifting airfoil. The convergence history shows the mean rate of change of the density and also the total number of supersonic points in the flow, which is almost immediately frozen in all these calculations. The pressure distribution of the RAE 2822 airfoil converged in only 25 cycles. Convergence was slower for the NACA 0012 airfoil. In the case of flow at Mach 0.8 and 1.25-deg angle of attack, additional cycles were needed to damp out a wave downstream of the weak shock wave on the lower surface.

As a further check and verification of accuracy, the drag coefficient should be zero in subsonic flow or in shock-free transonic flow. Table 2 shows the computed drag coefficient with the H-CUSP schemes on a sequence of three meshes for three examples. The first two are subsonic flows over the RAE 2822 and NACA 0012 airfoils at Mach 0.5 and 3-deg angle of attack. The third is the flow over the shock-free Korn airfoil at its design point of Mach 0.75 and 0-deg angle of attack. In all three cases the drag coefficient is calculated to be zero to four digits on a 160×32 mesh. In aeronautical applications the accurate prediction of drag is particularly important, and an error as large as 0.0005 is significant because the total drag coefficient of the wing of a transport aircraft (including friction, vortex, and shock drag) is in the range of 0.0150.

Three-Dimensional Calculations for a Swept Wing

To verify the properties of the H-CUSP scheme for three-dimensional problems, the flow past the ONERA M6 wing was calculated on a mesh with C-H topology and $192 \times 32 \times 48 = 294{,}912$ cells. Figure 3 shows the result at Mach 0.84 and 3.06-deg angle of attack. This verifies that the nonoscillatory character of the solution is preserved in three dimensions together with the sharp resolution of shock waves.

Flat-Plate Laminar Boundary Layer

A laminar boundary layer developing over a flat plate at zero incidence is generally chosen as the first test case to validate schemes for the viscous flow problems. In our case the computational domain is a rectangle with the inflow boundary located two plate lengths upstream of the leading edge and the downstream boundary located at the plate trailing edge. The upper boundary is located at a distance of four plate lengths. The mesh points are clustered in the streamwise direction near the leading edge to provide adequate resolution of the flow near the stagnation point. The finest grid contains a total of 512 cells in the streamwise direction with 384 cells placed along the plate. Within the boundary layer, the grid is equally spaced in the boundary-layer coordinate in the direction perpendicular to the plate. This ensures a constant level of resolution for all the boundary-layer profiles. It also ensures that an identical resolution is achieved independently of the Reynolds number. Outside of the boundary layer the grid is exponentially stretched toward the far field. The finest grid contains a total of 128 cells in the direction normal to the plate, half of which are within the boundary layer. Three coarser grids containing, respectively, 8, 16, and 32 cells within the boundary layer were obtained by elimination of alternate points, and they were used in the grid-refinement study.

Previous studies have shown that 32 cells are generally sufficient to resolve the viscous layer.[4] Figure 4 shows the result of a grid-refinement study on boundary-layer velocity profiles, which was carried out to investigate the accuracy of the cell-centered H-CUSP scheme. The numerical diffusion introduced by this scheme approaches zero as the local velocity approaches zero, and this scheme is therefore particularly suitable for the treatment of viscous boundary layers. All of the parameters of the numerical scheme are identical to those used for solving the Euler equations in the computation of the results presented in the preceding sections. A low value of the incoming flow Mach number ($M_\infty = 0.15$), well within the incompressible regime, was chosen to make a comparison with a Blasius solution meaningful.

Also, this flow condition tests the numerical scheme toward its limit of applicability as $M_\infty \to 0$, and the flow becomes incompressible. The Reynolds number of the incoming flow is 1×10^5. The results at four streamwise locations are overplotted to verify the self-similarity of the computed flow. It can be seen that both of the computed tangential and transverse components of the velocity follow the self-similarity law and give an excellent agreement with the Blasius solution even on the coarsest grid with eight cells in the boundary layer.

Although the errors, measured by the difference of the computed skin friction, displacement, and momentum thicknesses from the Blasius solution, decrease according to the grid refinement, their magnitude is less than 2% even in the case of the coarsest grid. With 32 cells in the boundary layer, the magnitude of the errors of the computed solution is less that 0.75% for all the quantities.

Two-Dimensional Turbulent Flows

The first set of calculations in this section is designed to validate the cell-centered H-CUSP scheme for a turbulent flow over a two-dimensional airfoil. The RAE 2822 test case 6 was selected.[5] Two meshes were used for the computations. The first consists of a total of 512×64 mesh cells with 385 points fitted on the airfoil, whereas in the second one the number of cells in the normal direction has been doubled to 128. The minimum distance from the airfoil surface of the first coordinate line is 2×10^{-5} chords, which corresponds to a value of $y^+ < 5$ for the assigned Reynolds numbers, and the outer boundary was placed at a distance of 18 chords. Transition was fixed at the experimental location of the trip wire. A Baldwin and Lomax turbulence model[6] has been used for this grid-refinement study because the flowfield was expected to be attached, and the behavior of the solution predicted by this model is reasonably well understood.

Figure 5 shows a comparison of the computed pressure coefficient along the airfoil for the two grid densities. The experimental results are also plotted as a reference. It can be seen that the computed pressure distribution is well converged on the 512×64 grid. The computed skin-friction coefficient, normalized by the freestream dynamic pressure, is also plotted in Fig. 5 and shows that grid-independent results are obtained on the 512×64 mesh.

Once the verification phase is concluded, the method is ready to be validated against independent experimental data. An example of validation presented next consists of an RC(4)-10 airfoil with a freestream Mach number of 0.59 and a Reynolds number of 7.5×10^6. The airfoil was designed for application to the inboard region of a helicopter main rotor blade.[7] This case was chosen to compare the prediction of the numerical scheme with independent experimental data. The turbulence model used here is again a simple algebraic Baldwin and Lomax. A C-type mesh consisting of a total of 512×64 mesh cells was used in the computations. The normal mesh spacing at the wall is 0.00002 chords, resulting in cells with aspect ratios on the order of 250:1 along the airfoil. Figure 6 shows a comparison of the surface pressure distribution between the computed result and the experimental data at an angle of attack of 3.41 deg. The agreement is very good, including the shock location. The agreement of computed lift, drag, and pitching moment with the experimental data, also very good over a wide range of angle of attack as it is, is shown in Fig. 6.

This calculation, therefore, contributes to the validation of the H-CUSP discretization for the simulation of attached viscous turbulent flows in the transonic regime.

Viscous Three-Dimensional Calculation for a Swept Wing

The next set of computations corresponds to the turbulent flow simulation on the ONERA M6 wing at $M = 0.84$, $Re = 11.7 \times 10^6$,

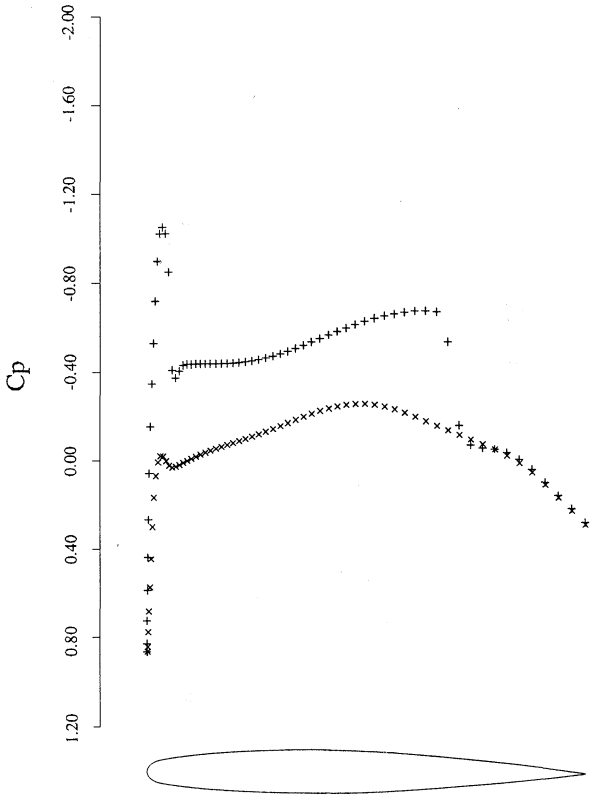

a) 12.50% span: C_l = 0.2933 and C_d = 0.0274

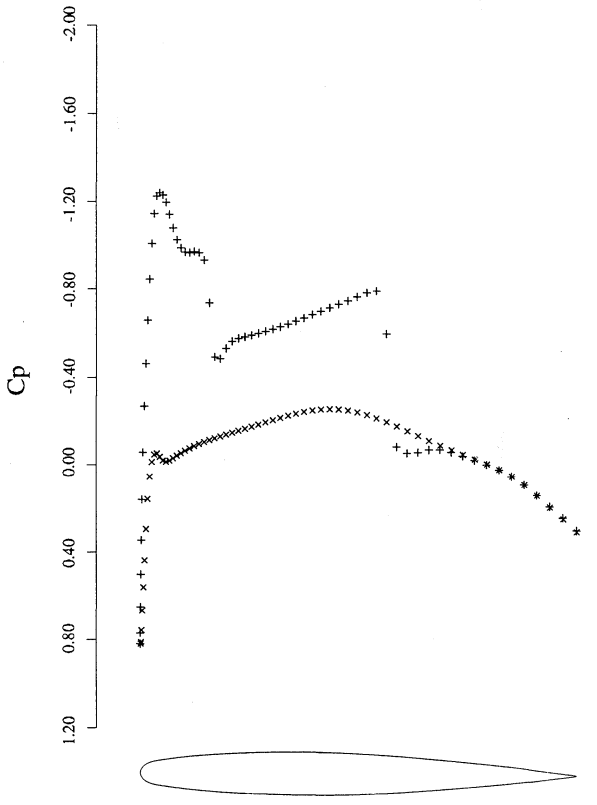

c) 50.00% span: C_l = 0.3262 and C_d = 0.0089

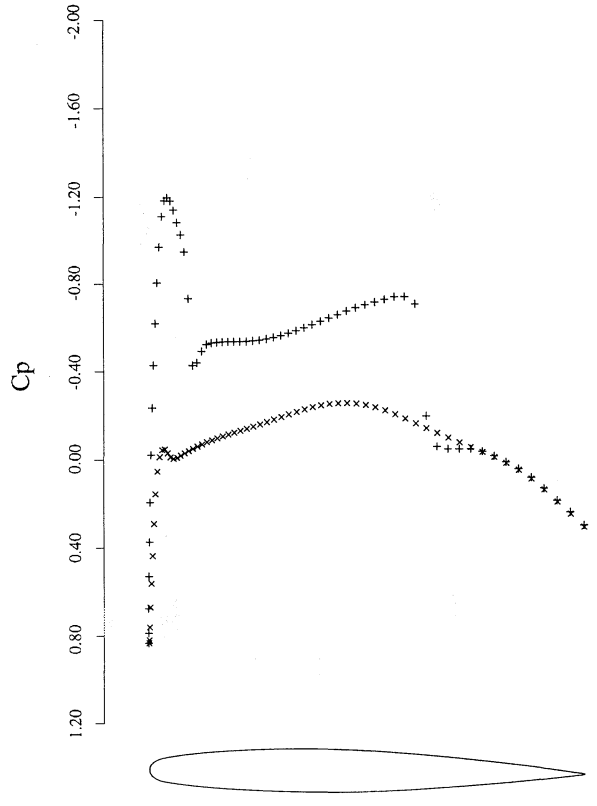

b) 31.25% span: C_l = 0.3139 and C_d = 0.0159

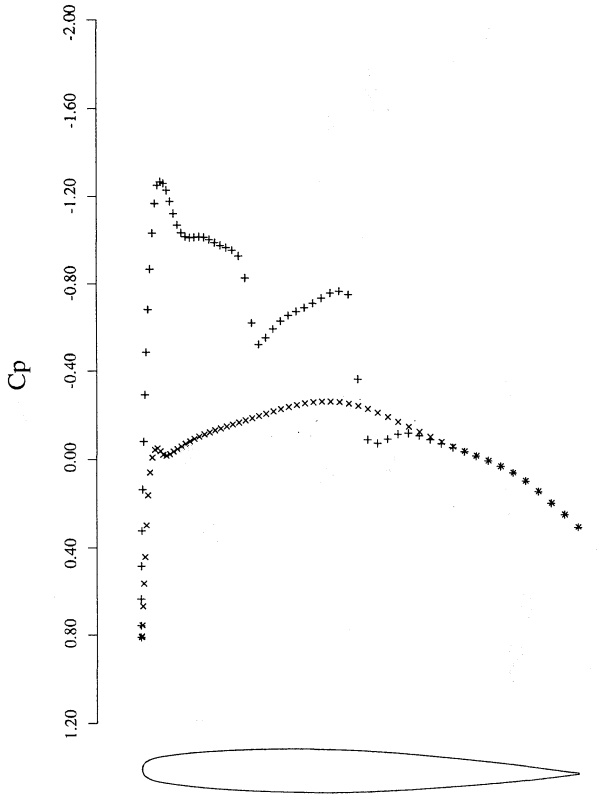

d) 68.75% span: C_l = 0.3195 and C_d = 0.0026

Fig. 3 Onera M6 wing: Mach 0.840, angle of attack 3.06 deg, 192 × 32 × 48 mesh, C_L = 0.3041, and C_D = 0.0131; H-CUSP scheme.

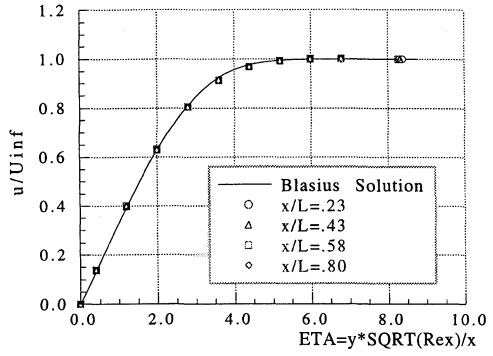

Tangential velocity, 8 cells in the layer

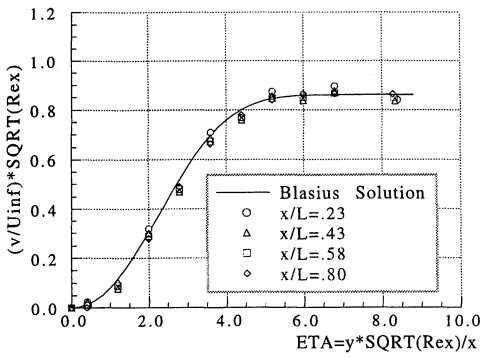

Transverse velocity, 8 cells in the layer

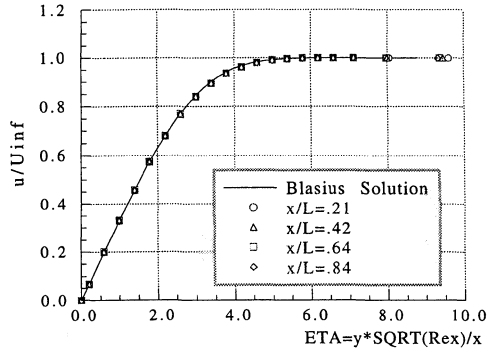

Tangential velocity, 16 cells in the layer

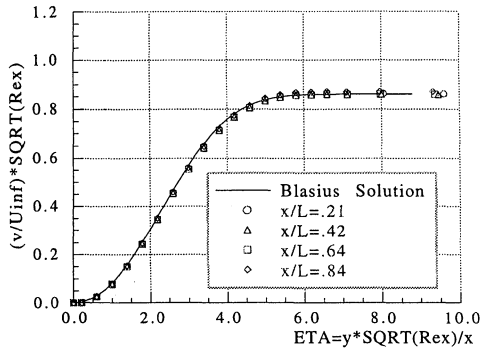

Transverse velocity, 16 cells in the layer

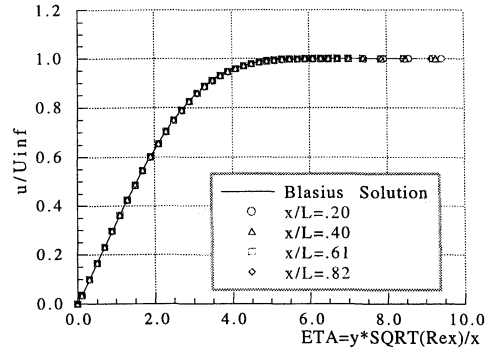

Tangential velocity, 32 cells in the layer

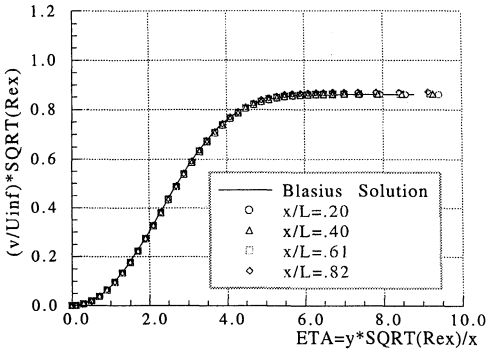

Transverse velocity, 32 cells in the layer

Fig. 4 Boundary-layer velocity profiles at $M = 0.15$ and $Re = 1 \times 10^5$.

and $\alpha = 3.06$ deg. The calculation was performed on a $193 \times 65 \times 49$ C-H grid using a vertex-based formulation of the H-CUSP scheme. A Johnson and King turbulence model was adopted. Figure 7 shows the comparison of measured and computed pressure coefficients at four stations along the span.

The agreement with the experimental data is reasonable for a mesh with only 614,705 mesh points. The computed lift and drag and the shock location compare favorably with the experiments, except at about the 80% of the span. There, the two inboard shocks merge, and a more accurate simulation would require an increased spanwise resolution. From the two-dimensional results we can infer that a $513 \times 65 \times 129$ grid may be needed for computing a grid-converged solution. Calculations of this size are only now becoming affordable. Thus, CFD methods for high-Reynolds-number viscous flow are still not validated as one would like before their use in the design process. In this case it becomes difficult to distinguish between the errors due to the mathematical model and those caused by the discretization, and care must be taken to isolate the cause of discrepancy either in the mathematical model or in the numerical scheme. Once again, grid-refinement studies will be instrumental for eliminating uncertainties and errors attributable to the numerical scheme.

Time-Resolved Incompressible Flow Simulations

The following sections present examples of the verification and validation of fully implicit time-stepping schemes that have been designed to allow the time step to be determined purely by accuracy requirements. In this approach, backward difference schemes of arbitrarily high order can be used to approximate the time derivatives. The second-order scheme is A-stable, whereas the third- and fourth-order schemes are stiffly stable. The implicit equations for a single time step are then solved by an inner time-stepping scheme with variable local time steps and multigrid acceleration.[8] This method has recently been extended for incompressible flows.[9] For this purpose, artificial compressibility is used in the inner time-stepping scheme. The first step in the development is the verification of the scheme by comparison with existing analytical results.

Oscillating Circular Cylinder in Incompressible Flow

The flow over a sinusoidally oscillating circular cylinder represents a good test for verification of numerical methods for inviscid incompressible flow. An analytic solution is known, and it provides a severe test for the computational algorithm because no physical dissipation is present. The diameter of a cylinder and a period of

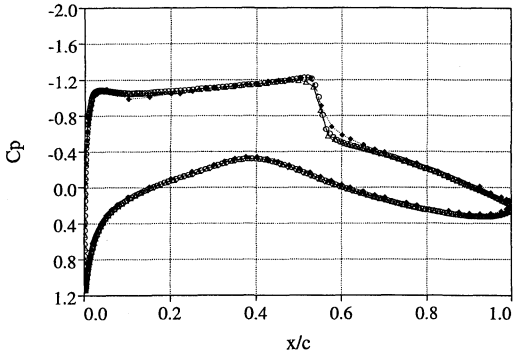

a) Computed pressure distribution: open triangles, 512 × 64 mesh; open circles, 512 × 128 mesh; and filled diamonds, experiments

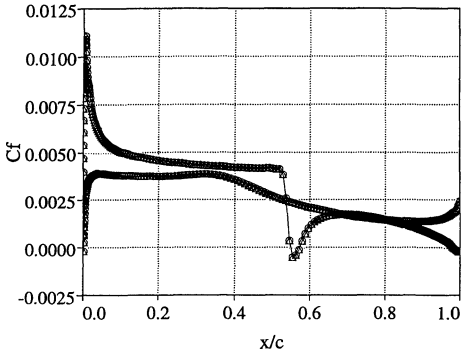

b) Computed skin friction: open triangles, 512 × 64 mesh, and open circles, 512 × 128 mesh

Fig. 5 Rae 2822 case 6, $M = 0.731$, $\alpha = 2.51$ deg, and $Re = 6.5 \times 10^6$.

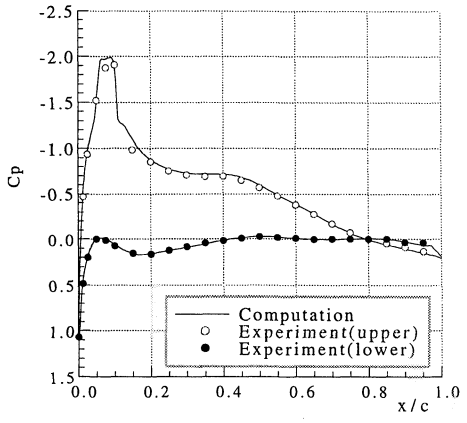

a) Pressure distribution: $M = 0.59$, $\alpha = 3.41$ deg, and $Re = 7.5 \times 10^6$

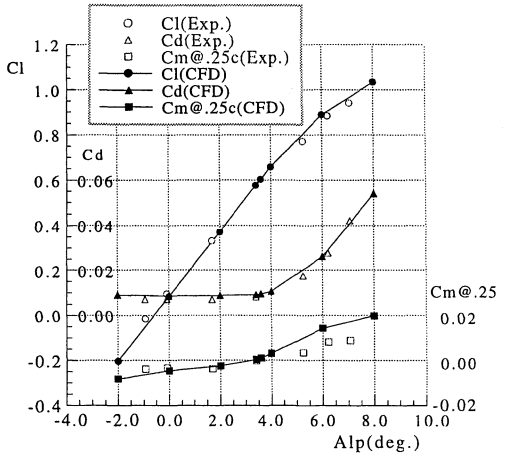

b) C_l, C_d, and C_m (0.25c): $M = 0.59$ and $Re = 7.5 \times 10^6$

Fig. 6 Comparison with experimental data for RC(4)-10 airfoil.

forced oscillations are chosen to be the length and the time scales of the problem, so that the nondimensional frequency f is equal to 1. The coordinate of the center of a cylinder is set to

$$x_{\text{cyl}}(t) = a \cdot \sin(\omega t - \varphi)$$

where the motion amplitude a is equal to 0.1 and the initial phase φ is 90 deg. The fluid velocity and the static pressure at infinity P_∞ are assumed to be zero. The exact solution for the incompressible inviscid flow over a moving cylinder can be found in the book by Landau and Lifshitz.[10] The velocity field and the surface pressure distribution reduce in this case to

$$u(\theta, t, r) = (0.25/r^2) \cdot u_{\text{cyl}}(t) \cdot \cos 2\theta$$

$$v(\theta, t, r) = (-0.25/r^2) \cdot u_{\text{cyl}}(t) \cdot \sin 2\theta \qquad (1)$$

$$P_s(\theta, t) = P_\infty + u_{\text{cyl}}^2(t) \cdot (2\cos^2\theta - 1.5) + \frac{\mathrm{d}u_{\text{cyl}}(t)}{2\,\mathrm{d}t} \cdot \cos\theta$$

where r is the distance to the center of a cylinder and θ is measured clockwise from the direction of the x axis. The third term in the pressure equation produces a nonzero net contribution to the dynamic drag force acting on a cylinder.

The resulting drag coefficient due to the apparent mass effect is

$$C_{d_{\text{cyl}}}(t) = (a\omega^2\pi/2) \cdot \sin(\omega t - \varphi) \qquad (2)$$

To verify the implicit scheme, a grid-refinement study was carried out using three O-meshes rigidly attached to the cylinder consisting of 65 × 33, 129 × 65, and 257 × 129 grid points, respectively.[9] The cylinder is initially at rest with $x_{\text{cyl}}(0) = -a$. The time step is $\Delta t = 0.025$, and the far-field boundary is placed 16 diameters away from the center of the cylinder. On each grid, the maximum modified residual in the divergence equation is reduced below 10^{-4} at each time step using approximately 50 multigrid W-cycles. The evolution of the drag coefficient computed on the 65 × 33 grid is compared in Fig. 8 with the exact solution [Eq. (2)], which is shown using a solid line. The calculation on the coarsest grid is found to overpredict the maximum drag amplitude by approximately 1.7%, whereas the results for the two finer grids coincide with the solid line. The order of convergence in the grid-refinement study can be estimated by the logarithm of the ratio of the computed drag amplitudes

$$\log_2\left[\frac{\max(C_{d_{65\times 33}}) - \max(C_{d_{129\times 65}})}{\max(C_{d_{129\times 65}}) - \max(C_{d_{257\times 129}})}\right] = 1.84$$

which is close to 2. This is indeed consistent with the second-order accuracy of the spatial discretization that was used. The pressure and velocity distributions on the surface of the cylinder, given by Eqs. (1), are plotted in Figs. 9–11. The comparison between the computed results and the analytical solution is excellent. This validates our numerical approach for inviscid incompressible flow.

Incompressible Vortex Shedding

For time-accurate calculations, a verification of the order of accuracy of the time-marching scheme is also necessary in addition to the standard verification of the accuracy in space. Thus it is a advisable to compute a given benchmark problem and compare the results computed with a sequence of progressively smaller time steps. The benchmark problem selected here is the parallel vortex shedding behind a half-cylinder corresponding to a Reynolds number of 2.5×10^2 based on the diameter. This is a very challenging and interesting problem that has been computed by other authors with a high-order spectral elements method.[11] When the integration is carried out for a long time, this flow exhibits a secondary instability leading to vortex pairing. Figure 12 shows the results of a time resolution study performed with a second-order accurate, A-stable backward difference scheme on a 192 × 384 O-mesh, with the far field located 45 diameters from the body. For this case, the shedding frequency is approximately 0.2. Thus, one full shedding cycle takes

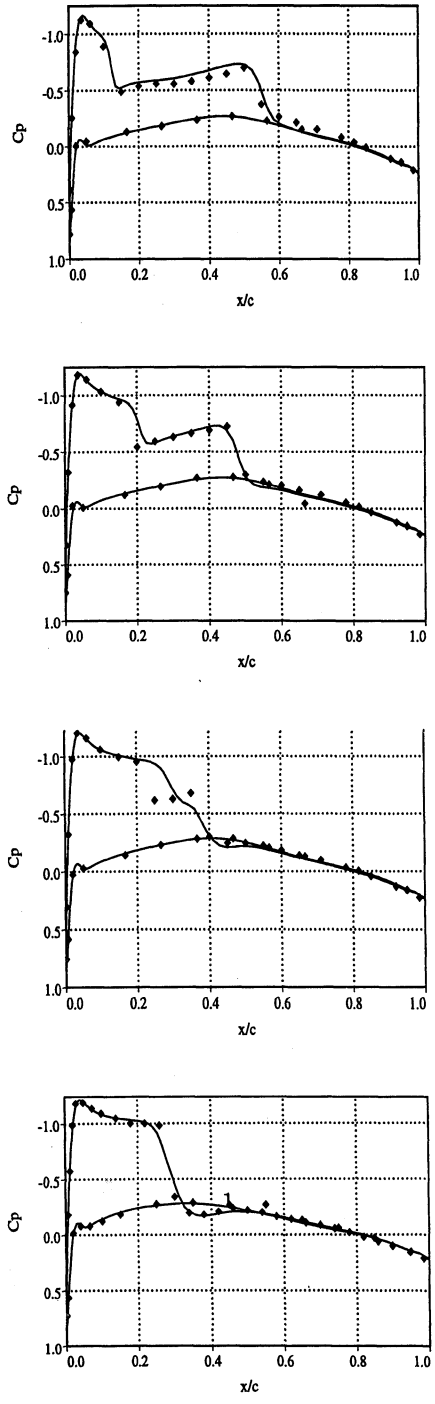

Fig. 7 Comparison of experimental and computed pressure coefficients for the ONERA M6 wing. Spanwise cuts at 0.44, 0.65, 0.80, and 0.90 (top to bottom): $M = 0.84, Re = 11.7 \times 10^6$, and $\alpha = 3.06$ deg.

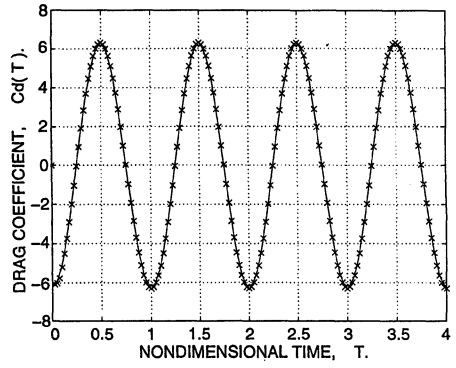

Fig. 8 Drag coefficient for an oscillating cylinder: Grid 65 × 33.

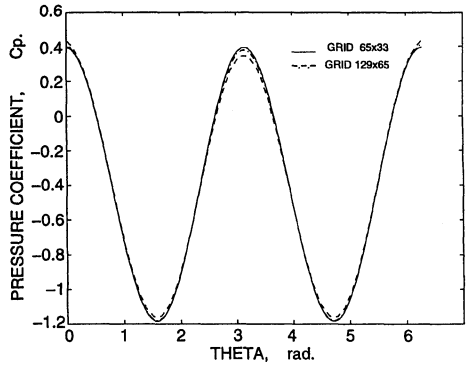

Fig. 9 Surface pressure coefficient for an oscillating cylinder, $t = 4.25$.

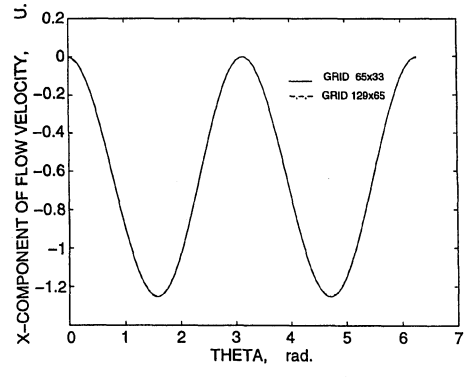

Fig. 10 Surface x component of the velocity for an oscillating cylinder, $t = 4.25$.

approximately 5 time units to complete. It is noted that the results obtained with $\delta t = \frac{5}{48}$—corresponding to 48 time steps per shedding cycle—almost overplot those obtained with a $\delta t = \frac{5}{96}$, indicating that convergence of the time approximation has been reached. When a third-order stiffly stable scheme is employed, the results for a time resolution study presented in Fig. 13 reveals that 48 time steps of the third-order scheme are sufficient to resolve one shedding cycle to the same accuracy as the most refined calculations with the second-order scheme.

Because in our implicit method the computational costs associated with increased time resolution reflect almost exclusively on memory, and not CPU, the net result of the time refinement study indicates a favorable tradeoff for the third-order-accurate scheme, which was then selected to carry out the final calculation of as many as 5000 shedding cycles necessary to observe the onset of the vortex pairing and to gather mean flow quantities. The results of that calculation, which are not reported here for the sake of brevity, were found to be in excellent agreement with the one obtained by using higher-order spectral methods. Thus, a study of time accuracy and a favorable comparison with the results computed by other authors with higher-order methods provide a solid verification of the overall method. The final validation step is described next.

The unsteady laminar vortex shedding from a circular cylinder for $Re \leq 3 \times 10^2$, based on the cylinder diameter and a freestream velocity, was selected a validation problem. This is a classical flow for which excellent experimental data at low Reynolds number are available. This shows that there is a sudden transition from two-dimensional parallel shedding to three-dimensional shedding. Recent experimental studies of the wake of circular cylinders[12] showed that a parallel shedding can be observed in the range of $4.9 \times 10^1 < Re < 1.8 \times 10^2$, provided that special care is taken to control the behavior of the flow at the ends of the cylinder. Above $Re = 1.8 \times 10^2$, three-dimensional shedding modes are observed, whereas for Reynolds numbers below 4.9×10^1 the wake is stationary.

For Reynolds numbers less than 1.5×10^2, the flow is essentially two dimensional. This allows the initial validation of the method to be carried out using a two-dimensional model. A 257×257 O-mesh

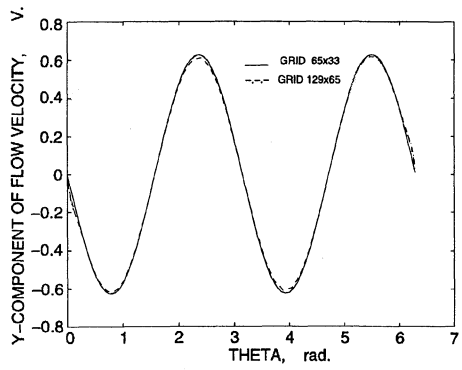

Fig. 11 Surface y component of the velocity for an oscillating cylinder, $t = 4.25$.

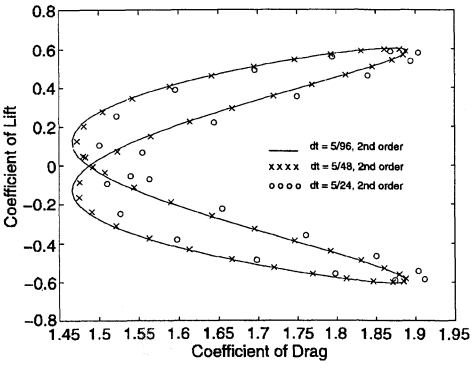

Fig. 12 Drag polar for a half-cylinder computed with a second-order-accurate scheme.

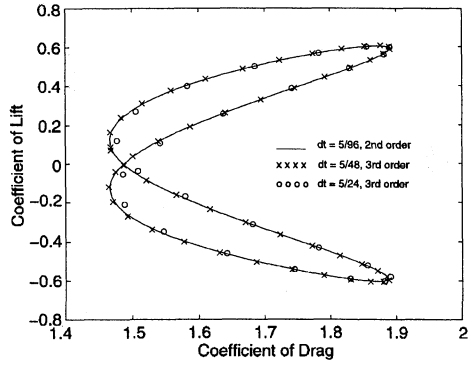

Fig. 13 Drag polar for a half-cylinder computed with a third-order-accurate scheme.

with a normal spacing of the grid next to the surface of 0.0003 diameters was used in the calculations. A relatively fine resolution of approximately 0.1 diameter is maintained in the radial direction up to the far-field boundary. The far-field boundary is placed at a distance of 16 diameters from the center of the cylinder.

The converged Strouhal frequency for $Re = 1.5 \times 10^2$ was found to be equal $Sr = 0.182$, whereas the values of the aerodynamic coefficients, corresponding to a limiting cycle, are $C_l = 0.000 \pm 0.486$ and $C_d = 1.168 \pm 0.025$. Once the asymmetric shedding developed, 15 multigrid W-cycles using seven grid levels were sufficient to enforce the divergence free constraint in each cell better than 10^{-5}.

To assess the effects of the spatial discretization, two auxiliary calculations with $Re = 1.5 \times 10^2$ are performed on two successively coarser grids with, respectively, 129×129 and 65×65 grid points. The coarser grids are constructed by eliminating the alternate points from the finest 256×256 grid, resulting in a somewhat lower resolution in the boundary layer. The order of convergence can be estimated using the ratios of the amplitudes of the oscillations of the aerodynamic coefficients as well as the Strouhal numbers computed on the three grids,

$$\log_2\left(\frac{Sr_{65\times 65} - Sr_{129\times 129}}{Sr_{129\times 129} - Sr_{257\times 257}}\right) = 2.27$$

$$\log_2\left[\frac{\max(C_{l_{65\times 65}}) - \max(C_{l_{129\times 129}})}{\max(C_{l_{129\times 129}}) - \max(C_{l_{257\times 257}})}\right] = 1.83$$

$$\log_2\left[\frac{\max(C_{d_{65\times 65}}) - \max(C_{d_{129\times 129}})}{\max(C_{d_{129\times 129}}) - \max(C_{d_{257\times 257}})}\right] = 2.01$$

which are indeed close to 2. This is consistent with the second-order accuracy of the spatial discretization and also is in agreement with the value obtained for the preceding inviscid calculations.

The laminar wake flow with $Re = 2 \times 10^2$ has been considered by many authors as a test case, and some of the relevant data, quoted from the literature, are presented in Table 3 (Refs. 11–18). However, according to Williamson and Roshko,[12] three-dimensional vortex shedding occurs at this Reynolds number. Also, the results in Ref. 11 suggest that the continuation of the universal curve corresponding to the parallel shedding (see the following analysis) and represented by the last entry in Table 3 might provide a better basis for validation of two-dimensional computations than the actual experimental data for this particular Reynolds number. Taking into account those considerations, and especially in view of the wide scattering of the data in Table 3, it appears that a lower Reynolds number flow ($Re = 1.5 \times 10^2$, for example) would provide a more meaningful validation of the two-dimensional numerical computations.

A continuous relation $Sr(Re)$ of the form

$$Sr(Re) = (A/Re) + B + C \cdot Re \tag{3}$$

where A, B, and C are constants, was proposed by Williamson[19] to describe the parallel vortex shedding believed to be accurate within 1%. The computed $Sr(Re)$ data for the set of calculations in the range of $Re \leq 2 \times 10^2$ are compared with the experimental curves and other computations[11–13] in Fig. 14. The curve-fitting coefficients, corresponding to Eq. (3), which were used for the comparison, are summarized in Table 4.

The experimental data of Williamson and Roshko[12] are shown in Fig. 14 for the range $4.9 \times 10^1 < Re < 1.8 \times 10^2$ by a solid line with the ticks indicating an estimated accuracy of ±1%. The results of our computational data are found to be in excellent—better than 1%—agreement with the universal curve in this range of Reynolds numbers.[19] Our data are also in good agreement with

Table 3 Flow over a circular cylinder at a Reynolds number of 2×10^2: coefficients of lift and drag and Strouhal number

	C_l	C_d	Sr
Present paper	±0.64	1.19 ± 0.041	0.196
Ref. no.			
14	±0.65	1.23 ± 0.05	0.185
15	±0.67	1.34 ± 0.043	0.196
16	±0.5	1.58 ± 0.0035	0.194
17	—	1.17	—
11	—	—	0.197
18	—	—	0.19
13 (exp.)	—	—	0.19
13 (fit.)	—	—	0.190
12 (fit.)	—	—	0.197

Table 4 Universal curve coefficients for the mean flow quantities in the wake of a circular cylinder

Ref. no.	Quantity	A	B	$C \times 10^4$
19	Sr	−3.3265	0.1816	0.1600
13	Sr	−4.50	0.212	—
11	Sr	−3.3658	0.1831	1.627
12	C_{pb}	−14.3500	0.6950	16.920
11	C_{pb}	−10.1090	0.6380	20.570

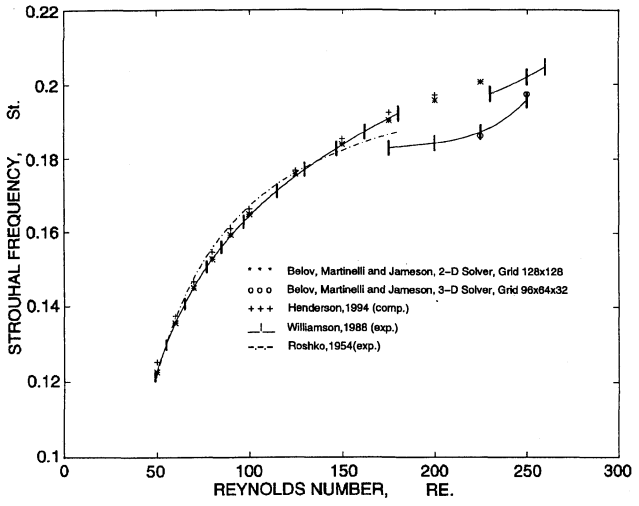

Fig. 14 Strouhal frequency as function of Reynolds number.

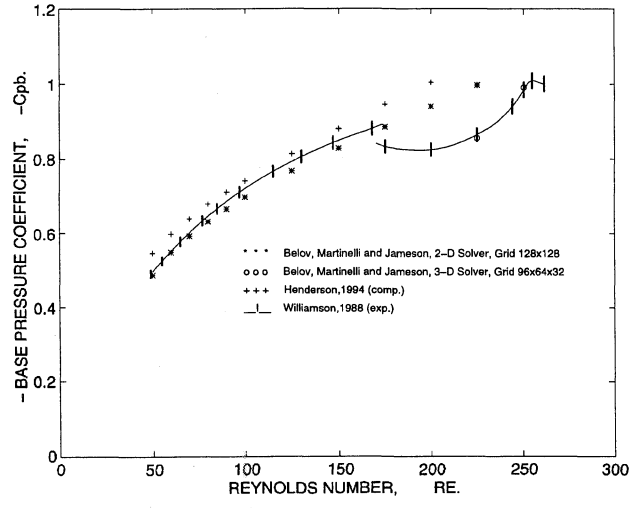

Fig. 15 Base pressure coefficient as function of Reynolds number.

the experimental curve obtained by Roshko[13] and the unstructured spectral element computations by Henderson.[11]

The computed variation of the base pressure coefficient with Reynolds number $C_{p_b}(Re)$ is shown in Fig. 15. Our data exhibit the same trend as other computational and experimental results,[11,13] yet they differ from the latter by 2 or 3%. This is within experimental errors. Below $Re < 4.9 \times 10^1$, the wake is stationary. A decaying response is observed in the calculations, confirming that the present method captures correctly the asymptotic behavior of wake flows for the range of Reynolds numbers considered.

To simulate the transition to three-dimensional shedding, three-dimensional computations were performed on a $96 \times 64 \times 32$ O-H-mesh for a cylinder with an aspect ratio $L/D = 6.4$. Periodic boundary conditions where imposed along the span. An initial disturbance was introduced in the flow to expedite the onset of the shedding. The results for $Re = 1.5 \times 10^2$ exhibit a decaying response to the initial disturbance and reach, asymptotically, a two-dimensional shedding, which is in agreement with the experimental predictions. At $Re = 2.25 \times 10^2$, the flow is unstable to the same disturbance: initially the flow develops essentially two-dimensional shedding, and then the $d(C_{p_b})$ and the maximum spanwise velocity component gradually increase by two orders in magnitude until a fully three-dimensional shedding is established. The time-averaged flow quantities corresponding to the initial parallel shedding regime agree reasonably well with those computed by the two-dimensional solver, as given in Table 4, despite the difference in spatial resolution of the two meshes. An identical behavior has been verified at $Re = 2.5 \times 10^2$. Thus, at least for the two Reynolds numbers computed, our model reproduces the expected transition from an initial parallel shedding to a fully three-dimensional regime, and the good agreement of both the computed Strouhal frequency and base pressure with the experimental data reinforces the validity of our numerical approach.

III. Conclusions

We believe that validation of computational methods is not simply a matter of comparing numerical results with experimental data. Rather, we see it as a complex multifaceted process in which every component step in the production of the final complete software needs to be separately verified and validated. One must begin by establishing that the mathematical model is logically consistent and that it is approximated by a correct numerical method, which is in turn implemented in a correct computer program. Only then can a comparison with experimental data be used to determine whether the mathematical model incorporates enough of the true physics to make useful predictions for the purpose in hand. Thus, each step in the process of developing the final complete software needs to be independently verified and validated in every feasible way. Mesh refinement studies provide guidance at every step of the process.

Once it is established by logical analysis and testing that the computational method does provide a sufficiently accurate solution of the intended mathematical model, one can proceed to assess the validity of the assumptions of the model by comparisons with experimental data. A fine enough mesh with a good enough quality must be used to ensure that there are not significant variations in the solution when either the number or the placement of the mesh points is varied. Otherwise it is impossible to distinguish modeling errors from numerical errors.

Acknowledgments

Our research has benefited greatly from the support of the Advanced Research Projects Agency under Grant N00014-92-J-1796, the Office of Naval Research under Grant N00014-93-I-0079, the Air Force Office of Scientific Research under Grant AFOSR-F49620-95-1-0259, and the Universities Space Research Association through the Research Institute for Advanced Computer Science at the NASA Ames Research Center. The support provided by an IBM-Cooperative Research Agreement grant is also gratefully acknowledged by the authors.

References

[1]Jameson, A., "Analysis and Design of Numerical Schemes for Gas Dynamics 1, Artificial Diffusion, Upwind Biasing, Limiters and Their Effect on Multigrid Convergence," *International Journal of Computational Fluid Dynamics*, Vol. 4, 1995, pp. 171–218.

[2]Jameson, A., "Analysis and Design of Numerical Schemes for Gas Dynamics 2, Artificial Diffusion and Discrete Shock Structure," *International Journal of Computational Fluid Dynamics*, Vol. 5, 1995, pp. 1–38.

[3]Roe, P. L., "Approximate Riemann Solvers, Parameter Vectors, and Difference Schemes," *Journal of Computational Physics*, Vol. 43, 1981, pp. 357–372.

[4]Martinelli, L., and Jameson, A., "Validation of a Multigrid Method for the Reynolds Averaged Equations," AIAA Paper 88-0414, Jan. 1988.

[5]Cook, P. H., McDonald, M. A., and Firmin, M. C. P., "Aerofoil RAE 2822 Pressure Distributions, Boundary Layer and Wake Measurements," AGARD, Advisory Rept. 138, 1979.

[6]Baldwin, B., and Lomax, H., "Thin Layer Approximation and Algebraic Model for Separated Turbulent Flow," AIAA Paper 78-257, 1978.

[7]Noonan, K. W., "Aerodynamic Characteristics of Two Rotorcraft Airfoils Designed for Application to the Inboard Region of a Main Rotor Blade," NASA-TP 3009, 1990.

[8]Jameson, A., "Time Dependent Calculations Using Multigrid, with Applications to Unsteady Flows Past Airfoils and Wings," AIAA Paper 91-1596, June 1991.

[9]Belov, A., Martinelli, L., and Jameson, A., "A New Implicit Algorithm with Multigrid for Unsteady Incompressible Flow Calculations," AIAA Paper 95-0049, Jan. 1995.

[10]Landau, L. D., and Lifshitz, E. M., *Fluid Mechanics*, 2nd ed., Butterworth Heinemann, Oxford, England, UK, 1987.

[11]Henderson, R. D., "Unstructured Spectral Element Methods: Parallel Algorithms and Simulations," Ph.D. Thesis, Princeton Univ., Princeton, NJ, June 1994.

[12]Williamson, C. H. K., and Roshko, A., "Measurements of Base Pressure in the Wake of a Cylinder at Low Reynolds Numbers Number Relationship for the Laminar Vortex Shedding," *Z. Flugwiss. Weltraumforsch*, Vol 14, 1990, pp. 38–46.

[13]Roshko, A., "On the Development of Turbulent Wakes from Vortex Streets," NACA Rept. 1191, 1954.

[14]Rogers, S. E., and Kwak, D., "Upwind Differencing Scheme for the Time-Accurate Incompressible Navier–Stokes Equations," *AIAA Journal*, Vol. 28, No. 2, 1990, pp. 253–262.

[15]Miyake, T., Sakamoto, Y., Tokunaga, H., and Satofuka, N., "Numerical Solution of Incompressible Flow Using Two-Step, One-Stage Runge–Kutta Time Integration Scheme," 1st European Computational Fluid Dynamics Conf., Brussels, Belgium, Sept. 1992.

[16]Lecointe, Y., and Piquet, J., "On the Use of Several Compact Methods for the Study of Unsteady Incompressible Viscous Flow Round a Circular Cylinder," *Computers and Fluids*, Vol. 12, No. 4, 1984, pp. 255–280.

[17]Lin, C. L., Pepper, D. W., and Lee, S. C., "Numerical Methods for Separated Flow Solutions Around a Circular Cylinder," *AIAA Journal*, Vol. 14, No. 7, 1976, pp. 900–907.

[18]Kovasznay, L. S. G., "Hot-Wire Investigation of the Wake Behind Cylinders at Low Reynolds Numbers," *Proceedings of the Royal Society of London, Series A*, Vol. 198, No. 1053, 1949, pp. 174–190.

[19]Williamson, C. H. K., "Defining a Universal and Continuous Strouhal-Reynolds Number Relationship for the Laminar Vortex Shedding of a Circular Cylinder," *Physics of Fluids*, Vol. 31, 1988, pp. 2742–2744.

A. Plotkin
Associate Editor